Journal of Computational Physics 430 (2021) 110034

Contents lists available at ScienceDirect

Journal of Computational Physics

www.elsevier.com/locate/jcp

Entropic Fokker-Planck kinetic model

M. Hossein Gorji [a,*], Manuel Torrilhon [b]

[a] Ecole Polytechnique Fédérale de Lausanne (EPFL), CH-1015 Lausanne, Switzerland
[b] MATHCCES, Department of Mathematics, RWTH Aachen University, Schinkestrasse 2, D-52062 Aachen, Germany

ARTICLE INFO

Article history:
Received 19 February 2020
Received in revised form 2 November 2020
Accepted 23 November 2020
Available online 30 November 2020

Keywords:
Fokker-Planck equation
Rarefied gas flows
DSMC
Monte-Carlo
Boltzmann equation

ABSTRACT

The diffusion limit of kinetic systems has been subject of numerous studies since prominent works of Lebowitz *et al.* [1] and van Kampen [2]. More recently, the topic has seen a fresh interest from the rarefied gas simulation perspective. In particular, Fokker-Planck based kinetic models provide novel approximations of the Boltzmann equation, where the relaxation induced by binary collisions is modeled via continuous stochastic processes. Hence in contrast to direct simulation Monte-Carlo, computational particles follow seemingly independent stochastic paths. As a result, a significant computational gain at small/vanishing Knudsen numbers can be obtained, where the dynamics of particles is overwhelmed by collisions. The cubic Fokker-Planck equation derived by [3] gives rise to the correct viscosity and Prandtl number for monatomic gases in the hydrodynamic limit, and further accurate behavior at moderate Knudsen numbers. Yet the model lacks a rigorous structure and more crucially does not admit the H-theorem. The latter underpins its accuracy e.g. in predicting shock wave profiles. This study addresses bridging the gap between diffusion processes and the Boltzmann equation by introducing the Entropic-Fokker-Planck kinetic model. The drift-diffusion closures derived for the model, allow for an H-theorem besides honoring consistent relaxation of moments. The devised model is validated with respect to direct simulation Monte-Carlo for high-Mach as well as Couette flows. Good performance of the model together with its easy to compute coefficients, makes the Entropic-Fokker-Planck framework attractive for computational investigation of gases beyond equilibrium.

1. Introduction

Gas flows in small scale devises or rarefied conditions may depart significantly from thermal equilibrium, and thus the conventional Navier-Stokes-Fourier equations fail to describe them properly. The Boltzmann equation on the other hand, gives the appropriate starting point for studying gas flows at such scenarios by providing a statistical account of molecular interactions. However, due to the complexity of the Boltzmann collision operator and high dimensionality of its solution domain, alternative computational methods are desirable. In general, three categories of solution methods tackle gas flows far from equilibrium.

Moment methods consider a finite set of partial differential equations (PDEs) governing the evolution of several velocity moments. The closure for higher order moments can be achieved by prescribing the distribution function or its expansion with respect to some basis. For example in the R13 method, the Grad distribution is employed for deriving the closures

* Corresponding author.
E-mail address: mohammadhossein.gorji@epfl.ch (M.H. Gorji).

https://doi.org/10.1016/j.jcp.2020.110034

(see e.g. [4–7]). Apart from relatively low computational cost, the moment methods can provide interesting insights about the physical mechanisms involved in high Knudsen gas flows. Yet inherent closure assumptions and complexity of boundary conditions are major drawbacks.

In particle Monte-Carlo methods, the flow field is described by computational particles representing the distribution function. Foremost, direct simulation Monte-Carlo (DSMC) invented by [8] is employed for rarefied gas flow simulations. As a particle Monte-Carlo scheme, it has been shown that the molecular distribution obtained by a converged DSMC simulation is consistent with solution of the Boltzmann solution [9,10]. Over its half-a-century development, DSMC has evolved to a mature general-purpose particle algorithm capable of dealing with complex rarefied gas flow scenarios [11]. Yet since collisions have to be resolved, DSMC can become prohibitively expensive at vanishing Knudsen numbers. The scenario which may arise e.g. in plume flows where a wide range of Knudsen numbers exists in the flow field. Another computational drawback comes from statistical errors associated with Monte-Carlo. In particular at the vanishing Mach number, the uncertainty of computed observables diverges. Recent advancements in DSMC techniques are thus tackling these issues; see e.g. [12,13].

The third category belongs to direct methods, where the PDE governing the evolution of the probability density is directly addressed. This can be applied either to the Boltzmann equation or to kinetic models with simpler operators such as BGK [14], S-BGK [15] or ES-BGK [16]. The main advantage of this category is that the computations are free from statistical noise. However the drawback comes from the high dimensionality of the solution domain. Efficient direct schemes have been devised e.g. based on the discrete velocity model or spectral methods (see [17,18]).

The stiffness of the collision operator which results in massive computational costs in the near-hydrodynamic/hydrodynamic regimes, can be treated by passing to the diffusion limit of the Boltzmann equation. In this context, the Fokker-Planck equation naturally arises as a diffusion approximation of the underlying Master equation. There has been an extensive amount of work on the Fokker-Planck limit of the Boltzmann equation e.g. see [1,2,19–22]. Lebowitz et al. [1] have analyzed the Fokker-Planck model for liquids based on studies of Kirckwood [23]. Pawula [19] and van Kampen [2] pursued Fokker-Planck type truncations applied to the (linearized) Boltzmann equation, using Kramers-Moyal and power size expansion, respectively. Bogomolov [21] obtained the Fokker-Planck limit of jump processes using the central limit theorem on the basis of Skorokhod theorem [20]. Heinz has introduced a Langevin model of the particle acceleration to address the Prandtl number issue [22].

Due to the inherent connection between white-noise driven stochastic processes and the Fokker-Planck equation, particle Monte-Carlo solution algorithms can be easily constructed upon Fokker-Planck kinetic models. From the computational point of view, the idea has been originally persuaded by [24], where the Langevin equation was employed for modeling particles kinetics. The Fokker-Planck model (FP) can be regarded as an approximation of the Botlzmann equation, where the effect of binary collisions is described by a drift-diffusion mechanism. In other words, the net force acting on a particle due to successive collisions is decomposed into a part which is correlated to the particles velocity (drift) and the remainder which is a purely random contribution (diffusion). The latter can be seen as a direct consequence of the molecular chaos and is responsible for entropy production (hence the H-theorem). Yet the drift and diffusion coefficients employed in the Fokker-Planck model are unclosed terms that should be determined based on the underlying collision operator. Matching evolution of different moments of the Boltzmann equation with those arising from the Fokker-Planck model, leads to closure equations for drift and diffusion coefficients.

The linear drift model proposed in [24], could only provide one time scale which can be found based on the relaxation of the stress tensor (i.e. second order velocity moment), and thus resulting in wrong Prandtl number of 3/2. Next, a cubic ansatz was derived by [3] where higher order terms were introduced in the drift term in order to match the relaxation of the heat-fluxes to those resulting from the Bollzmann collision integral. Since then different attempts were made in order to study the performance of cubic Fokker-Planck based kinetic model in more details [25]. Besides algorithmic improvements [26,27], the model was extended to a hybrid framework in order to cover a larger Knudsen number range [28,29].

Alternative Fokker-Planck models were proposed for studying rarefied gas flow simulations [21,30–32]. Bogomolov has devised a Fokker-Planck model based on hard-sphere collisions [21]. Mathiaud & Mieussens have introduced an Ellipsoidal Fokker-Planck model (ES-FP) where the diffusion coefficient incorporates non-equilibrium part of the pressure tensor as well [30]. Fei & Fang proposed an information preserving particle method based on the Fokker-Planck equation [31]. Singh & Ansumali achieved a Prandtl number correction in the Fokker-Planck model employing gradients of macroscopic variables [32]. In particular the ES-FP model devised by [30] had been compared with respect to the cubic-FP one [33]. The comparison suggests that the former gives more accurate shock profiles while the latter provides a better heat-transport prediction in the low Knudsen regime. Further studies are required in order to compare the performance of different Fokker-Planck models in more general settings. However note that all the above-mentioned Fokker-Planck models are limited to a specific molecular interaction law (mostly Maxwell interaction) and intrinsically limited in terms of the number of moments that they can match with the Boltzmann equation.

Motivated by recent studies pointing out to the lack of H-theorem and practical deficiency of the cubic-FP model in accurately resolving shock profiles [34,35], the objective of this work is to derive a mathematically rigorous FP framework which offers two features: consistency of moment relaxations and H-theorem.

In the following, first we review linear- and cubic- FP models. Next, theoretical limitations of the cubic-FP model, including lack of the H-theorem are discussed. In the follow up section, the Entropic Fokker-Planck (EFP) equation is introduced. Here an explicit relation between diffusion and drift coefficients is derived such that the positivity of the entropy production

is guaranteed. In Sec. 6, the solution algorithm and corresponding integration schemes are reviewed. In the results section, the Couette scenario as well as a high Mach flow of argon over a vertical plate is studied using the EFP model. The paper closes with concluding remarks.

2. Review of cubic-Fokker-Planck model

Consider a dilute gas medium with the density field $\rho(x,t)$. The molecular velocity distribution $\mathcal{F}=\rho f(v;x,t)$ corresponds to the probability density f of finding a molecule with a velocity infinitesimally close to $v\in\mathbb{R}^3$ at position $x\in\mathbb{R}^3$ and time $t\in\mathbb{R}^+$. Adopting the molecular chaos assumption, the Boltzmann equation

$$\frac{\partial\mathcal{F}}{\partial t}+\frac{\partial}{\partial x_i}(v_i\mathcal{F})=\frac{1}{m}\int_{\mathbb{R}^3}\int_0^{4\pi}\left(\mathcal{F}(v')\mathcal{F}(v_t')-\mathcal{F}(v)\mathcal{F}(v_t)\right)gI(\Omega,g)d\Omega dv_t \tag{1}$$

provides the evolution of $\mathcal{F}$ due to binary collisions of the form $(v,v_t)\rightarrow(v',v_t')$. Here g is the magnitude of the relative velocity $g=|v-v_t|$, $I(\Omega,g)$ is the differential cross section with Ω the solid angle about g, and m is the molecular mass. For details of the derivation see e.g. [36]. Here and henceforth the index summation convention is used for simple indices. Note that the right hand side of Eq. (1) will be denoted as S^{Boltz}. One of the issues in gas flow simulations based on the Boltzmann equation is the stiffness of the collision operator at low Knudsen numbers. For example in DSMC, the number of collisions that have to be calculated becomes significantly large as $\mathrm{Kn}\rightarrow 0$. Therefore an approximation that reduces the jump process arising from binary collisions to a continuous Markovian one, is highly attractive. A generic form of continuous Markovian processes is governed by the FP equation

$$\frac{\partial\mathcal{F}}{\partial t}+\frac{\partial}{\partial x_i}(v_i\mathcal{F})=\frac{\partial}{\partial v_i}(-A_i\mathcal{F})+\frac{\partial}{\partial v_iv_j}(D_{ij}\mathcal{F}) \tag{2}$$

with drift A and diffusion D [37]. In general, the FP operator is nonlinear with respect to $\mathcal{F}$ due to the fact that A and D are functions of $\mathcal{F}$. We refer to the right hand side of Eq. (2) as S^{FP}.

The physical assumption underlying the FP approximation can be better understood by considering a point particle following the random process generated by Eq. (2). The velocity of this particle continuously changes due to two contributions. One comes from the drift which is the summation of all forces correlated with the particle velocity. The other is the rapidly changing random force scaled by the diffusion. Note that the latter is an alternative account of the molecular-chaos and is a necessary means for the entropy production in the FP formulation.

The consistency between FP and Boltzmann operators has to be fulfilled by appropriate closures for drift and diffusion coefficients. Different degrees of consistency lead to different FP models with varying levels of complexity.

2.1. Linear drift

The simplest relevant closure is known as the Langevin equation. The closure for the drift

$$A_i=-\frac{1}{\tau}(v_i-U_i) \tag{3}$$

is a linear relaxation of the velocity towards the mean velocity U. The time scale $\tau=2\mu/p$ is chosen such that the viscosity μ will be achieved in the hydrodynamic limit. The pressure $p=nkT$ follows the ideal gas law (due to the dilute gas assumption) with number density n and temperature T.

Accordingly, the diffusion coefficient is found from energy conservation

$$D_{ij}=\frac{\theta}{\tau}\delta_{ij}, \tag{4}$$

where $\theta=kT/m$. Equations (3)-(4) lead to the following consistency relations

$$\int_{\mathbb{R}^3}\mathcal{P}S^{FP}dv=\int_{\mathbb{R}^3}\mathcal{P}S^{Boltz}dv \tag{5}$$

for $\mathcal{P}\in\{1,v_i,v_iv_j\}$, assuming the Maxwell interaction law. Note that while the higher order moments will have similar evolution forms in both operators, the relaxation rates are different. For example considering the heat-fluxes

$$q_i=\frac{1}{2}\int_{\mathbb{R}^3}v_i'v_j'v_j'\mathcal{F}dv, \tag{6}$$

the linear-drift FP model gives rise to the relaxation rate of $3p/(2\mu)$ which deviates from the rate $2p/(3\mu)$ resulting from the Boltzmann operator (with Maxwell molecules). Therefore a wrong Prandtl number of 3/2 is found in the hydrodynamic limit from the linear drift FP model.

The linear-drift FP model was adopted for rarefied gas flow simulations by [24]. Accurate mass flow rate results could be achieved for planar Poiseuille setup up to order one Knudsen numbers. Furthermore, its consistency with the second law of thermodynamics and thus the H-theorem has already been proven by [38]. However in order to tackle a wider range of problems, the Prandtl number issue had to be coped with.

2.2. Cubic drift

The relaxation of velocity moments in accordance with the Boltzmann operator can be obtained by a polynomial expansion of the drift. Therefore the drift was extended to a cubic form

$$A_i = c_{ij} v'_j + \gamma_i \left(v'_j v'_j - 3\theta \right) + \Lambda \left(v'_i v'_j v'_j - \frac{2q_i}{\rho} \right) \tag{7}$$

with the fluctuating velocity $v' = v - U$ [3]. The coefficients c and γ are introduced in order to match the evolution of second and third order velocity moments. Therefore they are found from the consistency relation

$$\int_{\mathbb{R}^3} \mathcal{P} S^{FP} dv = \int_{\mathbb{R}^3} \mathcal{P} S^{Boltz} dv; \quad \mathcal{P} \in \{1, v_i, v_i v_j, v_i v_j v_j\}, \tag{8}$$

where $\mathcal{P}$ is now extended to include the heat-fluxes as well. Consequently, the coefficients c and γ are found at each position and time from a 9×9 linear system of moments. The coefficient Λ is set to a small negative value (which vanishes at the equilibrium), for stability of the process. Finally, a diffusion closure similar to the Langevin model i.e. Eq. (4) was adopted. The cubic-FP model introduced by [3], has been studied for various rarefied gas flow problems including lid-driven cavity and high Mach flows [25,28]. While accurate results could be achieved in different test cases, certain formal and practical problems arise due to the extension given by Eq. (7).

3. Limitations of cubic-Fokker-Planck

In this section we analyze some theoretical shortcomings of the cubic-FP model.

3.1. H-theorem

Let us consider the evolution of the entropy functional

$$\mathcal{H}(\mathcal{F}) = -\int_{\mathbb{R}^3} \mathcal{F} \log \mathcal{F} dv \tag{9}$$

for the FP equation (2) in a homogeneous setting. Therefore

$$\frac{\partial \mathcal{H}}{\partial t} = \int_{\mathbb{R}^3} \frac{\partial A_i}{\partial v_i} \mathcal{F} dv + \int_{\mathbb{R}^3} \frac{D_{ij}}{\mathcal{F}} \frac{\partial \mathcal{F}}{\partial v_i} \frac{\partial \mathcal{F}}{\partial v_j} dv. \tag{10}$$

Now by applying the cubic-FP closure

$$\frac{\partial \mathcal{H}}{\partial t} = \overbrace{\rho \left(c_{ii} + 15\theta\Lambda \right)}^{\dot{\mathcal{H}}_A} + \overbrace{\frac{\theta}{\tau} \int_{\mathbb{R}^3} \frac{1}{\mathcal{F}} \frac{\partial \mathcal{F}}{\partial v_i} \frac{\partial \mathcal{F}}{\partial v_i} dv}^{\dot{\mathcal{H}}_D} \tag{11}$$

is obtained. For the Maxwellian distribution

$$\mathcal{F}_0 = \mathcal{Z}^{-1} \exp\left(-\frac{v'_i v'_i}{2\theta} \right) \tag{12}$$

the macroscopic coefficients become $c_{ij} = -\frac{1}{\tau}\delta_{ij}$, $\gamma_i = 0$ and $\Lambda = 0$. Therefore the right hand side of Eq. (2) vanishes and the equilibrium is achieved.

Yet for a general distribution $\mathcal{F}$, the entropy rate arising from the drift i.e. $(c_{ii} + 15\theta\Lambda)$ is not known explicitly. Therefore $d\mathcal{H}/dt$ might become negative depending on the ratio between $\dot{\mathcal{H}}_A$ and $\dot{\mathcal{H}}_D$. In a general setting, the cubic-FP model may not admit the H-theorem.

3.2. Time scale

The time scale τ in the cubic-FP model controls the diffusion and thus the entropy production rate $\dot{\mathcal{H}}_D$. However there is no clear justification for the value $\tau = 2\mu/p$ which is taken from the Langevin process. Note that for any positive τ, the system of constitutive equations arising from Eq. (8) lead to correct transport properties in the hydrodynamic limit. Therefore the notion of τ is somewhat redundant for the cubic model.

3.3. Stability

The cubic coefficient Λ was introduced in the drift in order to have a dominant attractive acceleration towards the mean velocity, as the fluctuations become large. Note that this stability argument is purely intuitive and has little or no mathematical justification. A more appropriate stability criterion can be sought from the kinetic equation (2). By providing the H-theorem, the solution of the FP equation becomes stable. Therefore in order to have a stable stochastic process, it would be sufficient to construct a FP equation which admits the H-theorem.

In the next section we introduce the Entropic-FP equation which overcomes the mentioned deficiencies.

4. Entropy guided Fokker-Planck expansion

4.1. General formulation

Consider a class of FP equations

$$\frac{\partial}{\partial t}\mathcal{F} = \frac{\partial}{\partial v_i}\left(\frac{\partial \Psi}{\partial v_i}\mathcal{F}\right) + D\frac{\partial^2}{\partial v_i \partial v_i}\mathcal{F} \tag{13}$$

where the drift $A_i = -\partial\Psi(\mathbf{v}, t, \mathcal{F})/\partial v_i$, and the diffusion $D_{ij}(\mathbf{v}, t, \mathcal{F}) = D(t, \mathcal{F})\delta_{ij}$ may depend on $\mathcal{F}$. Before proceeding to the details of the closure for Ψ and D, below we sketch the main idea behind the above kinetic model.

Let

$$J_l = \left\{ \alpha = (\alpha_i, 1 \le i \le 3) \,\middle|\, \alpha_i \in \{0, 1, ..., l\}, |\alpha| = \sum_{i=1}^{3} \alpha_i \right\} \tag{14}$$

for $l = 1, 2, ...$, denote the set of multi-indices α. Now consider a series of FP operators

$$S^{FP,l}(\mathcal{F}) = \frac{\partial}{\partial v_i}\left(\frac{\partial}{\partial v_i}\Psi^{(l)}\mathcal{F}\right) + D^{(l)}\frac{\partial^2}{\partial v_i \partial v_i}\mathcal{F}, \tag{15}$$

where $\Psi^{(l)}$ is such that for a given l and for $\forall \alpha \in J_l$, we get

$$\int_{\mathbb{R}^3} S^{FP,l}(\mathcal{F}) H_\alpha(v')dv = \overbrace{\int_{\mathbb{R}^3} S^{Boltz}(\mathcal{F}) H_\alpha(v')dv}^{\dot{P}_\alpha}, \tag{16}$$

where $\{H_\alpha\}_{\alpha \in J_\alpha}$ are $|\alpha|$-order rotational invariant Hermite polynomials. By fulfilling Eq. (16), Hermite projections of the solution of the FP equation become identical to the ones arising from the Boltzmann equation. Hence assuming that solutions of both equations admit Hermite expansions, the solution of the FP equation (if it exists) converges to the solution of the Boltzmann equation in the weighted L^2 sense [39].

Consequently the question of the FP kinetic model reduces to devising Ψ and D such that the resulting FP equation has a solution and Eq. (16) is fulfilled for a given order l. A general approach to achieve that is by considering a Hermite expansion of Ψ for a given $l \in \mathbb{N}$

$$\Psi^{(l)}(c, v') = \sum_{\alpha \in J_l} c_\alpha H_\alpha(v') \tag{17}$$

and a non-negative value for the diffusion. Once $D^{(l)}$ is fixed, the coefficient vector c can be found from linear equations resulting from Eq. (16). More clearly let

$$S_{\alpha\beta} = \int_{\mathbb{R}^3} \frac{\partial}{\partial v_i} H_\alpha \frac{\partial}{\partial v_i} H_\beta \mathcal{F} dv \quad \text{and} \tag{18}$$

$$L_\alpha = \int_{\mathbb{R}^3} \frac{\partial^2 H_\alpha}{\partial v_i \partial v_i}\mathcal{F} dv. \tag{19}$$

Therefore

$$c_\alpha = \sum_{\beta \in J_l} S^{-1}_{\alpha\beta} \left(D^{(l)} L_\beta - \dot{P}_\beta \right). \tag{20}$$

Observe that $S_{\alpha\beta}$ is a symmetric-positive-definite matrix. Furthermore, $\dot{P}_\alpha$ are given by the Boltzmann collision operator. They have a closed form structure for Maxwell's interaction law and can be approximated for other potentials [40]. Note that $D^{(l)}$ is responsible to control the entropy of the solution, whose closure is discussed in the following.

4.2. Entropy consideration

An important property of the Boltzmann operator is the H-theorem. Physically, it means that the entropy of the system is increased through collisions. Mathematically, the H-theorem provides the L^1 regularity in terms of the distance from the equilibrium, through Kullback's inequality [41]. Therefore providing an H-theorem can also lead to the long-time solution existence of the FP equation. Below first we derive a relationship between Ψ and D which results into the H-theorem. Next we provide drift-diffusion closures in accordance with the entropy constraint.

4.2.1. H-theorem

First we should find a condition such that the Maxwellian distribution becomes the stationary solution of Eq. (13). However note that Eq. (20) with $\mathcal{F} = \mathcal{F}_0$ yields $\Psi^{(l)} = 1/2 D^{(l)} v_i' v_i'/\theta$. Therefore no extra constraint on Ψ and D would be required to keep the solution stationary at the Maxwellian.

Now let us move to the non-equilibrium scenario. First observe the entropy evolution

$$\frac{\partial \mathcal{H}}{\partial t} = \int_{\mathbb{R}^3} \left(-\frac{\partial^2 \Psi^{(l)}}{\partial v_i \partial v_i} + D^{(l)} \frac{\partial}{\partial v_i} \log \mathcal{F} \frac{\partial}{\partial v_i} \log \mathcal{F} \right) \mathcal{F} dv. \tag{21}$$

In the following we justify that the constraint

$$D^{(l)}_{opt} = \dot{\mathcal{H}}_\Psi, \tag{22}$$

where

$$\dot{\mathcal{H}}_\Psi = \frac{\theta}{3\rho} \int_{\mathbb{R}^3} \frac{\partial^2 \Psi^{(l)}}{\partial v_i \partial v_i} \mathcal{F} dv \tag{23}$$

ensures $\partial \mathcal{H}/\partial t \geq 0$. Using $\mathcal{F}_0$ given by Eq. (12), we have

$$\begin{aligned} \int_{\mathbb{R}^3} \left(-\frac{\partial^2 \Psi^{(l)}}{\partial v_i \partial v_i} + D^{(l)}_{opt} \frac{\partial}{\partial v_i} \log \mathcal{F} \frac{\partial}{\partial v_i} \log \mathcal{F} \right) \mathcal{F} dv &= -\frac{3\rho}{\theta} D^{(l)}_{opt} + D^{(l)}_{opt} \left(\frac{3\rho}{\theta} + \right. \\ &\left. \int_{\mathbb{R}^3} \mathcal{F} \frac{\partial}{\partial v_i} \log \frac{\mathcal{F}}{\mathcal{F}_0} \frac{\partial}{\partial v_i} \log \frac{\mathcal{F}}{\mathcal{F}_0} dv \right) \\ &= \int_{\mathbb{R}^3} \mathcal{F} \frac{\partial}{\partial v_i} \log \frac{\mathcal{F}}{\mathcal{F}_0} \frac{\partial}{\partial v_i} \log \frac{\mathcal{F}}{\mathcal{F}_0} dv, \end{aligned} \tag{24}$$

see Appendix A for details. Now using Eq. (22), we get

$$\frac{\partial \mathcal{H}}{\partial t} = D^{(l)}_{opt} \int_{\mathbb{R}^3} \mathcal{F} \frac{\partial}{\partial v_i} \log \frac{\mathcal{F}}{\mathcal{F}_0} \frac{\partial}{\partial v_i} \log \frac{\mathcal{F}}{\mathcal{F}_0} dv \tag{25}$$

and hence $\partial \mathcal{H}/\partial t \geq 0$ with equality for $\mathcal{F} = \mathcal{F}_0$.

4.2.2. Diffusion closure

The constraint (22) suggests a closure for $D^{(l)}$. In fact provided $\dot{\mathcal{H}}_\Psi \geq 0$, Eq. (22) yields

$$D^{(l)}_{opt} = \frac{-\sum_{\alpha,\beta \in J_l} S^{-1}_{\alpha\beta} \dot{P}_\alpha L_\beta}{3\rho/\theta - \sum_{\alpha,\beta \in J_l} S^{-1}_{\alpha\beta} L_\alpha L_\beta}, \tag{26}$$

by virtue of Eq. (20), and thus $\partial \mathcal{H}/\partial t \geq 0$ is obtained. However since the right hand side of Eq. (26) can become negative, the closure may fail to exist. Yet one key observation here is that the negative value of $\dot{\mathcal{H}}_\Psi$ (which corresponds to negative

values of the right hand side of Eq. (26)), leads to $\partial\mathcal{H}/\partial t \geq 0$. The latter can be easily checked from Eq. (21). Using this fact, we propose the closure

$$D^{(l)} = \left| \frac{\sum_{\alpha,\beta\in J_l} S^{-1}_{\alpha\beta}\dot{P}_\alpha L_\beta}{3\rho/\theta - \sum_{\alpha,\beta\in J_l} S^{-1}_{\alpha\beta} L_\alpha L_\beta} \right| \tag{27}$$

for the diffusion coefficient, which is positive and yields

$$\frac{\partial\mathcal{H}}{\partial t} \geq 0 \tag{28}$$

irrespective of the sign of $\dot{\mathcal{H}}_\psi$, as shown in the following. First observe that

$$\frac{\partial\mathcal{H}}{\partial t} = -\frac{3\rho}{\theta}\dot{\mathcal{H}}_\Psi + D^{(l)} \int_{\mathbb{R}^3} \mathcal{F}\frac{\partial}{\partial v_i}\log\mathcal{F}\frac{\partial}{\partial v_i}\log\mathcal{F} dv. \tag{29}$$

Now let us consider two cases

1. Suppose we have

$$\frac{\sum_{\alpha,\beta\in J_l} S^{-1}_{\alpha\beta}\dot{P}_\alpha L_\beta}{3\rho/\theta - \sum_{\alpha,\beta\in J_l} S^{-1}_{\alpha\beta} L_\alpha L_\beta} \leq 0 \Rightarrow \dot{\mathcal{H}}_\Psi \geq 0, \tag{30}$$

   and hence the inequality (28). In other words, this scenario corresponds to the case where $D^{(l)} = D^{(l)}_{opt}$ and therefore Eq. (25) holds.
2. Consider the case when

$$\frac{\sum_{\alpha,\beta\in J_l} S^{-1}_{\alpha\beta}\dot{P}_\alpha L_\beta}{3\rho/\theta - \sum_{\alpha,\beta\in J_l} S^{-1}_{\alpha\beta} L_\alpha L_\beta} \geq 0 \Rightarrow \dot{\mathcal{H}}_\Psi \leq 0. \tag{31}$$

   Observe that since $\dot{\mathcal{H}}_\Psi \leq 0$, the inequality (28) is fulfilled due to Eq. (29).

We refer to the FP equation with closures (17) and (27) as the EFP model.

4.2.3. Discussion

Before proceeding to an affordable EFP model, it is important to explore the closure given by Eq. (27) in more details.

1. Observe that we have

$$\sum_{\alpha,\beta\in J_l} S^{-1}_{\alpha\beta}\dot{P}_\alpha L_\beta \to 0 \quad \text{and} \quad \sum_{\alpha,\beta\in J_l} S^{-1}_{\alpha\beta} L_\alpha L_\beta \to \frac{3\rho}{\theta}$$

   as $\mathcal{F}\to\mathcal{F}_0$. Therefore it is necessary to make sense of Eq. (27) at $\mathcal{F}=\mathcal{F}_0$. By interpreting the equilibrium via $\lim_{\epsilon\to 0}\mathcal{F}_0(1+\epsilon\Phi(v'))$, the limit of Eq. (27) can be evaluated for a polynomial $\Phi(.)$. Yet in practice we don't need to evaluate Eq. (27) at the equilibrium (limit), since any pair of $(\Psi^{(l)} = 1/2D^{(l)}v_i'v_i'/\theta, D^{(l)} > 0)$ yields $S^{FP,l}(\mathcal{F}_0) = 0$.
2. While both discussed cases 1 and 2 provide non-negative entropy productions, the former is the preferred one due to two reasons. First, note that the entropy rate of the former case is proportional to the Fisher information

$$\mathcal{I}(\mathcal{F}|\mathcal{F}_0) = \int_{\mathbb{R}^3} \mathcal{F}\frac{\partial}{\partial v_i}\log\frac{\mathcal{F}}{\mathcal{F}_0}\frac{\partial}{\partial v_i}\log\frac{\mathcal{F}}{\mathcal{F}_0} dv. \tag{32}$$

   The Fisher information is a measure of uncertainty and induces a metric between two distributions with fundamental importance in many physical systems [42,43]. Second, the condition $\dot{\mathcal{H}}_\Psi \leq 0$ implies that the drift is gradient of a scalar which is convex in the average sense. This can have favorable consequences in terms of the stability of the random paths generated by the resulting FP equation.

5. Quadratic entropic Fokker-Planck model

Now based on the general EFP formulation, we propose a computationally affordable model. In order to achieve correct transport properties (i.e. viscosity and heat conductivity) we focus only on the evolution of moments up to the heat-fluxes. Hence the consistency relations reduce to

$$\int_{\mathbb{R}^3} S^{FP,(3)}(\mathcal{F}) H_\alpha(v') dv = \int_{\mathbb{R}^3} S^{Boltz}(\mathcal{F}) H_\alpha(v') dv \tag{33}$$

where $H_\alpha \in \{1, v'_i, 1/2 v'_k v'_k, v'_i v'_j - 1/3 v'_k v'_k \delta_{ij}, v'_i v'_j v'_j\}$. Accordingly, the potential ansatz takes the form

$$\Psi = c_i^{(1)} v'_i + \frac{1}{2} c_{ll}^{(2)} v'_k v'_k + c_{ij}^{(2)} \left(v'_i v'_j - \frac{1}{3} v'_k v'_k \delta_{ij} \right) + c_i^{(3)} v'_i v'_j v'_j. \tag{34}$$

5.1. Closures

Note that the first order term $c^{(1)}$ can be found from the rest, due to conservation of momentum

$$c_i^{(1)} = -3 c_i^{(3)} \theta - 2 c_j^{(3)} \frac{p_{ij}}{\rho}, \tag{35}$$

where $p_{ij} = \int_{\mathbb{R}^3} v'_i v'_j \mathcal{F} dv$. Furthermore, only the symmetric part of $c_{ij}^{(2)}$ is relevant. Therefore we end up with nine unknowns (six $c^{(2)}$ and three $c^{(3)}$). The corresponding equations for $c^{(2,3)}$ can be written more transparently using the following notation. Let

$$x = \left[\tilde{c}_{11}^{(2)} \; \tilde{c}_{12}^{(2)} \; \tilde{c}_{13}^{(2)} \; \tilde{c}_{22}^{(2)} \; \tilde{c}_{23}^{(2)} \; \tilde{c}_{33}^{(2)} \; \tilde{c}_1^{(3)} \; \tilde{c}_2^{(3)} \; \tilde{c}_3^{(3)} \right]^T, \tag{36}$$

where $\tilde{c}$ is comprised of the unknowns in the drift

$$A_i = \tilde{c}_{ij}^{(2)} v'_j + \tilde{c}_i^{(3)} \left(v'_j v'_j - 3\theta \right) + 2 \tilde{c}_j^{(3)} \left(v'_i v'_j - \frac{p_{ij}}{\rho} \right) \tag{37}$$

and is a function of c according to

$$\tilde{c}_{ij}^{(2)} = -\left(c_{ij}^{(2)} + c_{ji}^{(2)} \right) - \frac{1}{3} c_{ll}^{(2)} \delta_{ij} \tag{38}$$

$$\text{and} \quad \tilde{c}_i^{(3)} = -c_i^{(3)}. \tag{39}$$

Furthermore, let y be the production vector $\dot{P}_\alpha$. Therefore the consistency relations can be written in the form

$$\mathcal{L}_{ij} x_j = y_i - D z_i \tag{40}$$

where $z = \rho[1\ 0\ 0\ 1\ 0\ 1\ 0\ 0\ 0]^T$. An explicit form of $\mathcal{L}$ is given in Appendix B. Hence we have

$$D = \left| \frac{\mathcal{L}_{jk}^{-1} y_k z_j}{3\rho/\theta - \mathcal{L}_{pq}^{-1} z_p z_q} \right| \tag{41}$$

$$\text{and} \quad x_i = \mathcal{L}_{ij}^{-1} \left(y_j - D z_j \right). \tag{42}$$

The production terms $\dot{P}_\alpha$ should be specified from the underlying molecular law. Except the case of Maxwell interactions, they do not have an analytical form unless a closure for the distribution is prescribed. In this study we adopt the non-linear production terms evaluated by [40] for the case of hard sphere interaction law.

5.2. Discussion

The drift-diffusion closures given by Eqs. (37) and (41) give rise to a quadratic Entropic FP model (referred henceforth as quad-EFP) which admits the H-theorem subject to a constrained relaxation of moments up to the heat-fluxes. In comparison to the cubic-FP model, the EFP formulation does not require stabilizing term due to the fact that the entropy constraint bounds the L^1 distance of the distribution from the equilibrium. Furthermore in contrast to the other kinetic models such as ES-FP or ES-BGK, the EFP formulation does not depend on a specific structure of the production term $\dot{P}$. Therefore generalization for complex molecular potentials and/or including higher order moments are rather straight-forward. Note that the quad-FP algorithm would not introduce any extra computational cost compared to the cubic-FP model. Besides particles state time-stepping, the algorithm only needs to invert a 9×9 coefficient matrix $\mathcal{L}$ (similar to cubic-FP). All the rest of model coefficients are given explicitly.

In the following Section, we discuss a numerical integration scheme for the quad-EFP model in a particle framework very similar to the cubic-FP scheme.

6. Solution algorithm

Similar to DSMC, a particle Monte-Carlo technique is developed in order to perform simulations based on the quad-EFP model. Itô's Lemma provides us with the set of stochastic processes that represent the same distribution as the solution of the Fokker-Planck equation [37,44]. More precisely suppose $M(t) - X(t)$ are time-indexed velocity-position processes governed by

$$dM_i(t) = A_i dt + D dW_i \quad \text{and} \tag{43}$$

$$dX_i = M_i dt, \tag{44}$$

where dW_i is the Wiener process honoring $\langle dW_i \rangle = 0$ and $\langle dW_i dW_j \rangle = dt\delta_{ij}$ with $\langle \ldots \rangle$ the ensemble average. As it is derived by [45], the probability density of realizations generated by the above stochastic differential equations (SDEs) (43)-(44) converges to $f(V; x, t)$ being the solution of the Fokker-Planck equation (2) with $D_{ij} = D\delta_{ij}$.

By examining the SDEs (43)-(44), the motivation behind the Fokker-Planck kinetic model becomes more evident. Here each stochastic path generated by the process only depends on the moments of the distribution function. Thus providing an accurate integration scheme one can overcome the high cost of dense collisions appearing in the near-hydrodynamic regime [28].

6.1. Time integration

The time integration scheme devised for the cubic-FP model [25] can be readily applied to the quad-EFP model. The idea is to make use of the exact integration of the Langevin equation together with a first order approximation of the nonlinear contribution in the drift. Moreover, fluctuating velocities are scaled such that kinetic energy is conserved. In order to formulate the same scheme here, we have to introduce a relevant time scale for decomposition of the process into a Langevin part and the remainder. We can do this by defining a frequency

$$\nu = \frac{D}{\theta} \tag{45}$$

and correspondingly

$$A_i = -\nu M'_i + N_i \tag{46}$$

where $M' = M - U$ and

$$N_i = \left(\tilde{c}^{(2)}_{ij} - \nu\delta_{ij}\right) M'_j + \tilde{c}^{(3)}_i \left(M'_j M'_j - \langle M'_j M'_j \rangle\right) + 2\tilde{c}^{(3)}_j \left(M'_j M'_i - \langle M'_j M'_i \rangle\right). \tag{47}$$

Let M^j and X^j be approximations of the velocity and position at time t^j resulting from the numerical scheme. Therefore velocity-position updates follow

$$M^{n+1}_i = \frac{1}{\alpha^n}\left(M'^{,n}_i e^{-\Delta t\nu^n} + (1 - e^{-\Delta t\nu^n})\frac{1}{\nu^n} N^n_i + D^n\sqrt{\frac{1}{\nu^n}(1 - e^{-2\Delta t\nu^n})}\xi_i)\right) + U^n_i \tag{48}$$

$$\text{and} \quad X^{n+1}_i = X^n_i + M^n_i \Delta t \tag{49}$$

for the time step size $\Delta t = t^{n+1} - t^n$. Note that all the values with the superscript n and $n+1$ are evaluated at t^n and t^{n+1}, respectively. Here ξ_i are independent standard normal variates. The conservation of energy is ensured by the correction factor α

$$\alpha^2 = 1 + \frac{1}{3D}\left(\nu^{-1}(1 - e^{-\Delta t\nu})^2 \langle N_i N_i \rangle + 2\left(e^{-\Delta t\nu} - e^{-2\Delta t\nu}\right)\langle M'_i N_i \rangle\right), \tag{50}$$

see [28] for details.

6.2. Moments

As a particle Monte-Carlo scheme, the moments of the distribution function are evaluated from an ensemble of particles (realizations). Consider a set of n_p particles in the infinitesimal volume $\delta\Omega(x)$ around point x at time t. Thus the distribution

$$\mathcal{F}(v, x, t) = \frac{1}{\delta\Omega} \lim_{n_p \to \infty} \sum_{j=1}^{n_p} \delta\left(M^{(j)}(t) - v\right) w^{(j)} \tag{51}$$

Table 1
Outline of the Algorithm.

1-	Move particles according to Eq. (49).
2-	Apply boundary conditions.
3-	Calculate coefficients per cell via Eq. (42) and Eq. (41).
4-	Update particles velocities based on Eq. (48).
5-	Sample observables.

can be represented by the set of particles velocities $M^{(j)}$ with $j \in \{1, ..., n_p\}$. The statistical weight $w^{(j)}$ is the number of real molecules that are simulated by particle j. Using a finite set of particles, the identity (51) becomes an approximation through which different moments of $\mathcal{F}$ can be estimated at each position from nearby particles.

Once different velocity moments are sampled from the particles, the macroscopic coefficients and the diffusion have to be estimated and then utilized in the update scheme (48)-(49). That involves solution of the system (42) and then evaluation of diffusion via (41).

6.3. Solution algorithm

Initially, the physical domain is discretized into a set of fine enough computational cells. The resolution requirement here is to capture the gradients of macroscopic quantities [26,46]. According to the CFL criterion, then the time step size is chosen. Note that both local grid refinement and local time stepping might be employed as well [27]. A minimum number of 20-50 particles per cell has to be considered if instantaneous averaging is conducted for estimating the coefficients involved in the drift and diffusion. Furthermore, treatment of boundary conditions is similar to other kinetic models. They are fully determined by the wall kernel or inflow/outflow distribution fluxes. In summary the algorithm is outlined in Table 1.

7. Results

Two sets of simulations are conducted for validation of the quad-EFP model. First, the planar Couette flow is studied at different Knudsen numbers. Next, the high Mach flow around a vertical plate is simulated. The focus in both simulations is to demonstrate the accuracy of the quad-EFP model. For all simulations, the hard sphere model of argon with $d = 3.628 \times 10^{-10}$ m and $m = 66.3 \times 10^{-27}$ kg is employed. Therefore, in both cubic-FP and quad-EFP simulations the macroscopic coefficients are found based on the Boltzmann production terms corresponding to the hard sphere model [40]. DSMC simulations are conducted based on Bird's algorithm [8].

7.1. Couette

The gas at the number density $n = 10^{20}$ $1/\text{m}^3$ is confined between two isothermal walls at $T_w = 273$ K moving with respect to each-other at the speed of $U_w = 300$ m/s. The channel is assumed to be long enough and therefore the flow condition only varies normal to the walls i.e. along the x-coordinate. The walls are separated by the distance L, where diffuse boundary condition is applied to both $x = 0$ and $x = L$. Three Knudsen numbers are considered $Kn = \lambda/L \in \{0.02, 0.1, 0.5\}$ with λ being the hard sphere mean-free-path. The flow domain $x = [0, L]$ is discretized into $n_{cell} = 200$ computational cells resulting in the length $\delta x = L/n_{cell}$ for each. According to the CFL criterion, the time step size $\Delta t = \delta x/\theta_w/2$ is utilized. Total number of 10^5 particles are employed in each simulation, which initially 5,000 time steps are calculated to reach the stationary condition; the time averaging is employed for 20,000 steps onwards. The results are calculated using quad-EFP, cubic-FP and DSMC. The mean velocity U and the temperature T are depicted in Fig. 1. Very good agreement between all three methods can be seen. The slip velocity and the temperature jump are captured accurately by the FP models. However as Kn increases, the discrepancy appears especially inside the Knudsen layer. Furthermore, a slight but clear improvement of the quad-EFP model with respect to the cubic-FP can be observed.

7.2. Flow over a plate

As a more challenging test case, Ma=5 flow of argon around a vertical plate of length $L = 0.1828$ m is considered. The physical domain is extended $2.5L$ along x- and $3L$ along y-axis. The upstream condition is set to $T_0 = 273$ K and $n_0 = 10^{20}$ $1/\text{m}^3$. The flow enters vacuum condition at the downstream $x = 2.5L$. Vertical ends of the domain i.e. $y = 0$ and $y = 3L$ are assumed to be specular boundaries. The isothermal plate is $1.25L$ far from the inflow and assumed to be diffusive with $T_w = 273$ K. The Knudsen number based on the half of the plate size is 0.14. Symmetry condition at $y = 1.5L$ is exploited and only the upper half of the domain is simulated. Therefore the computational domain $2.5L \times 1.5L$ is discretized into 120×120 computational cells resulting in $\Delta t = 1.5978 \times 10^{-6}$ s according to the CFL condition. Particles statistical weights are set to 4×10^{-13} kg resulting in around 3×10^6 number of particles at the stationary condition. Initially 2,000 time steps are advanced and afterward, 5,000 steps for time averaging.

Formation of a normal shock and its interaction with rarefaction waves from the tip of the plate at the downstream, make the flow structure quite complex. While the FP models produce smoother shocks, a better agreement between the

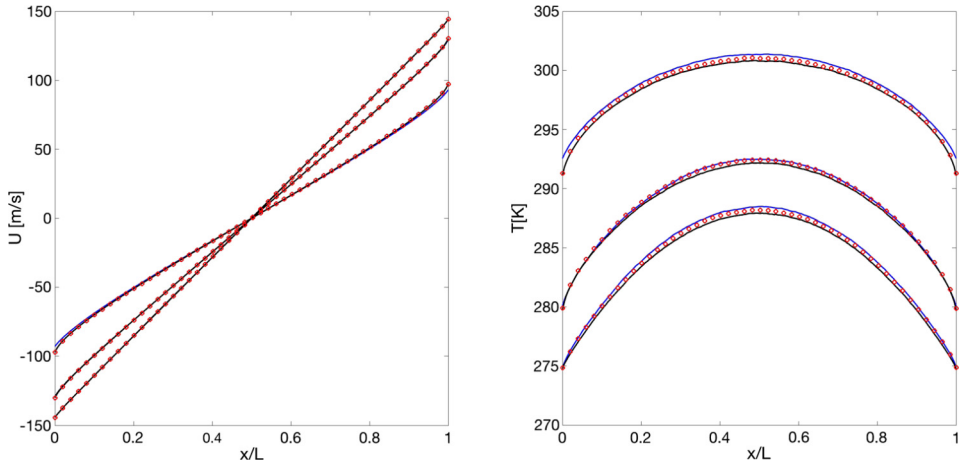

Fig. 1. Couette flow at Kn$\in \{0.02, 0.1, 0.5\}$; black: cubic-FP, red: quad-EFP and blue: DSMC; left: mean velocity $U[m/s]$ and right: temperature $T[K]$. (For interpretation of the colors in the figure(s), the reader is referred to the web version of this article.)

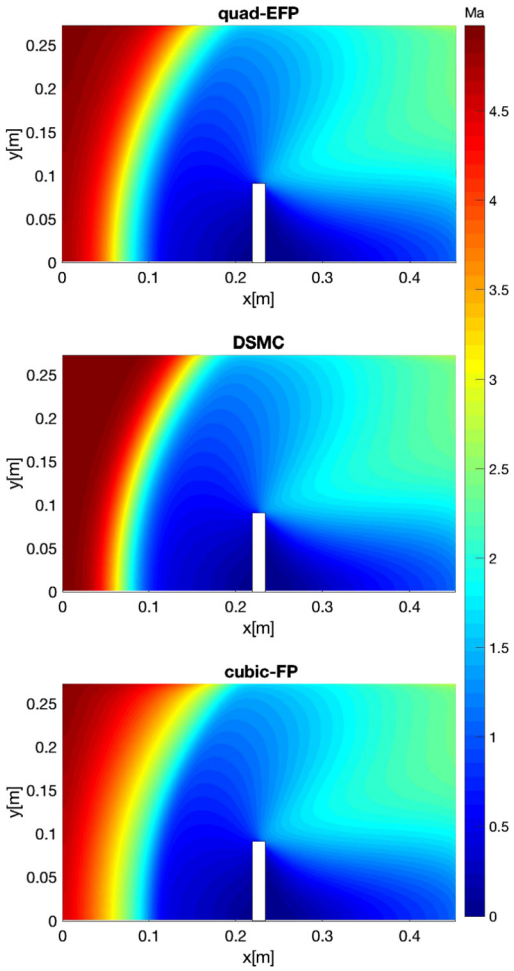

Fig. 2. Mach contours of supersonic flow of argon around a vertical plate at Kn=0.14. Results of quad-EFP, DSMC and cubic-FP are shown at top, middle and bottom, respectively.

quad-EFP model and DSMC can be observed in Mach contours depicted in Fig. 2. More detailed results are shown in Figs. 3 and 4 for different moments along $y = 1.875L$ line. Better agreements are shown between the quad-EFP model and DSMC.

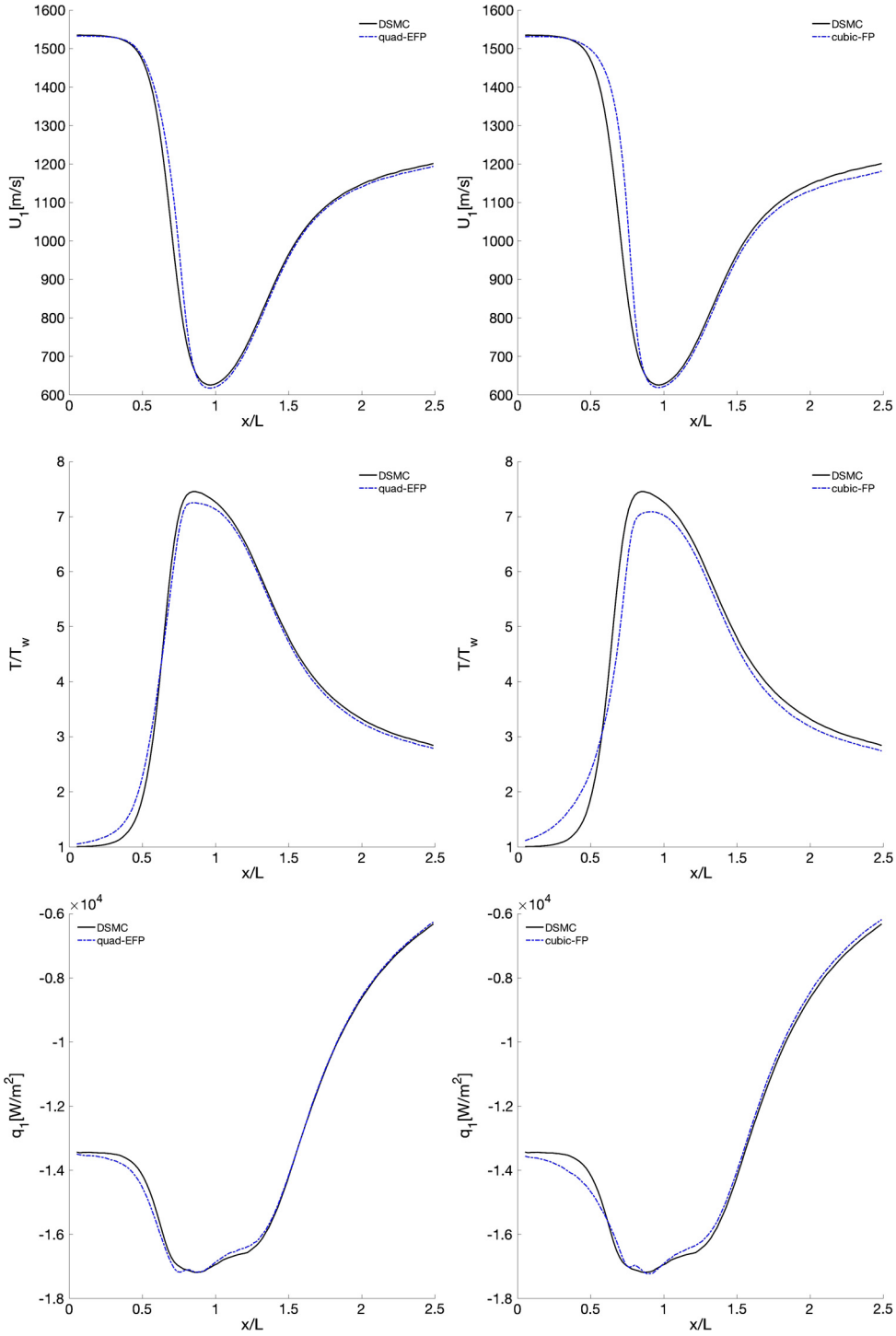

Fig. 3. $Ma = 5$ flow of argon around a vertical plate at Kn=0.14. The $x-$component of the bulk velocity i.e. $U_1[m/s]$, the normalized temperature T/T_w and the stream-wise heat-flux i.e. $q_1[W/m^3]$ are shown along $y = 1.875L$ at top, middle and bottom, respectively.

An insight into the EFP diffusion closure can be gained by looking at the ratio η between the quad-FP diffusion Eq. (42) and the cubic-FP diffusion Eq. (4). Let us examine the value of η in our planar shock problem based on the quad-FP simulation result. As evident from Fig. 5, the diffusion value of the quad-FP model is almost half of the corresponding cubic-FP diffusion in the shock region. Both diffusion coefficients become close to each other in the subsonic region near the flat plate. Furthermore it is interesting to see that the quad-FP diffusion adopts the favorable D_{opt} almost everywhere

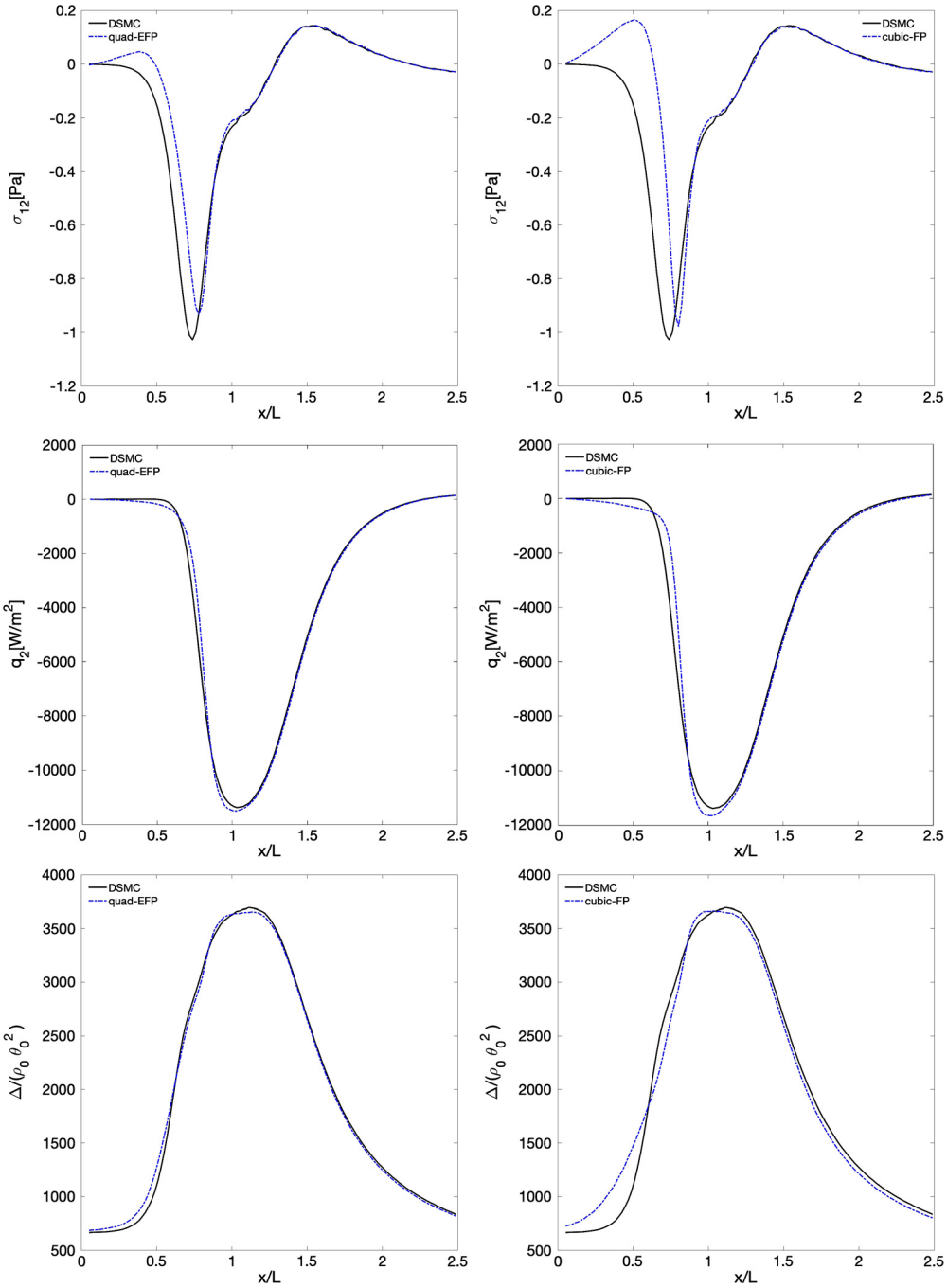

Fig. 4. $Ma = 5$ flow of argon around a vertical plate at Kn=0.14. The planar stress i.e. $\sigma_{12} = \int_{\mathbb{R}^3} v_1' v_2' \mathcal{F} dv$, the lateral heat-flux $q_2[W/m^3]$ and the fourth order moment $\Delta = \int_{\mathbb{R}^3} v_i' v_i' v_j' v_j' \mathcal{F} dv - 15p^2/\rho$ scaled by $\rho_0\theta_0^2$, are shown along $y = 1.875L$ at top, middle and bottom, respectively.

except inside the shock, where sharp gradients are observed. In other words, for the considered example the inequality $\dot{\mathcal{H}}_\psi \geq 0$ is violated only inside the shock.

8. Conclusion

In this work, we addressed the Fokker-Planck approximation of the Boltzmann equation following twofold objectives: moment consistency and entropy law. The former could be achieved by considering an expansion of the drift coefficient while the latter is honored by introducing an appropriate diffusion coefficient. The model offers attractive characteristics: fulfilling H-theorem, giving rise to correct moment relaxations (also in principle beyond heat-fluxes), linear system for

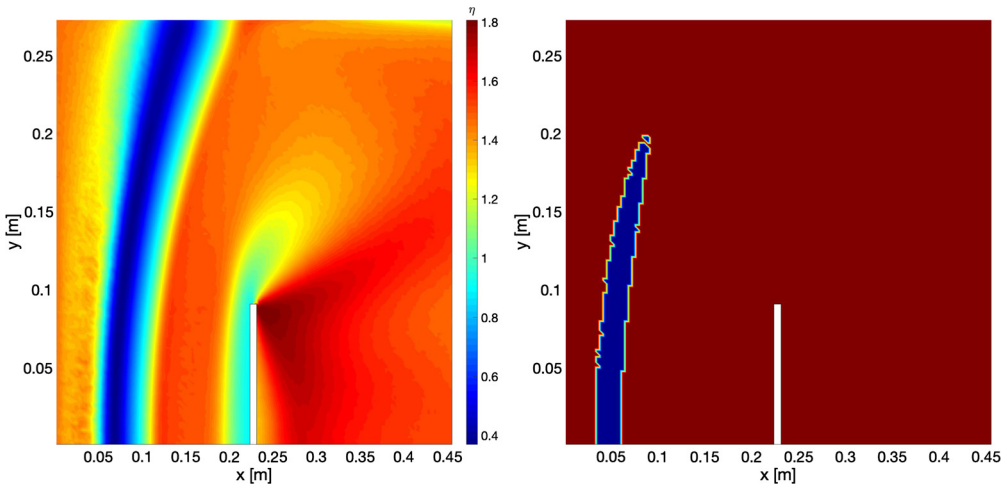

Fig. 5. $Ma = 5$ flow of argon around a vertical plate at Kn=0.14; left: diffusion ratio η; right: red denotes regions with $\dot{\mathcal{H}}_\psi \geq 0$ and blue denotes regions with $\dot{\mathcal{H}}_\psi < 0$.

the unknowns, and all that without relying on any free parameter. We believe that these characteristics already provide a crucial step towards general-purpose Fokker-Planck kinetic models. Therefore a simple quadratic drift Fokker-Planck model was derived which gives rise to correct relaxations of moments up to the heat-fluxes besides satisfying the H-theorem. The resulting quad-EFP model was then compared with respect to the cubic-FP model as well as DSMC. Overall a better agreement between quad-EFP and DSMC was found. It is interesting to see that no arbitrary time scale had to be introduced for the EFP formulation, and the model is fully determined by the Boltzmann collision integrals. Future studies will focus on the extension of the EFP model for polyatomic gases and mixtures.

CRediT authorship contribution statement

M. Hossein Gorji: Conceptualization, Methodology, Software, Validation, Writing – original draft. **Manuel Torrilhon:** Methodology, Supervision, Writing – review & editing.

Declaration of competing interest

The authors declare that they have no known competing financial interests or personal relationships that could have appeared to influence the work reported in this paper.

Acknowledgement

Hossein Gorji acknowledges the funding provided by Swiss National Science Foundation under the grant number 174060. The authors appreciate fruitful exchanges with Patrick Jenny and Julien Mathiaud on the Entropic Fokker-Planck closure.

Appendix A. Derivation of entropy rate

In this appendix, we provide justifications for the equality

$$\int_{\mathbb{R}^3} \frac{\partial}{\partial v_i} \log \frac{\mathcal{F}}{\mathcal{F}_0} \frac{\partial}{\partial v_i} \log \frac{\mathcal{F}}{\mathcal{F}_0} \mathcal{F} dv = \int_{\mathbb{R}^3} \mathcal{F} \frac{\partial}{\partial v_i} \log \mathcal{F} \frac{\partial}{\partial v_i} \log \mathcal{F} dv - \frac{3\rho}{\theta} \tag{A.1}$$

employed in derivation of Eq. (24). Similar derivations can be found e.g. in [38]. First note that

$$\begin{aligned} \int_{\mathbb{R}^3} \frac{\partial}{\partial v_i} \log \frac{\mathcal{F}}{\mathcal{F}_0} \frac{\partial}{\partial v_i} \log \frac{\mathcal{F}}{\mathcal{F}_0} \mathcal{F} dv = & \int_{\mathbb{R}^3} \mathcal{F} \frac{\partial}{\partial v_i} \log \mathcal{F} \frac{\partial}{\partial v_i} \log \mathcal{F} dv \\ & -2 \int_{\mathbb{R}^3} \mathcal{F} \frac{\partial}{\partial v_i} \log \mathcal{F} \frac{\partial}{\partial v_i} \log \mathcal{F}_0 dv \\ & + \int_{\mathbb{R}^3} \mathcal{F} \frac{\partial}{\partial v_i} \log \mathcal{F}_0 \frac{\partial}{\partial v_i} \log \mathcal{F}_0 dv. \end{aligned} \tag{A.2}$$

The second and third terms on the right hand side read

$$-2\int_{\mathbb{R}^3}\mathcal{F}\frac{\partial}{\partial v_i}\log\mathcal{F}\frac{\partial}{\partial v_i}\log\mathcal{F}_0 dv = -2\int_{\mathbb{R}^3}\frac{\partial}{\partial v_i}\mathcal{F}\frac{\partial}{\partial v_i}\log\mathcal{F}_0 dv$$
$$= 2\int_{\mathbb{R}^3}\frac{v_i'}{\theta}\frac{\partial}{\partial v_i}\mathcal{F}dv = -\frac{6\rho}{\theta} \tag{A.3}$$

and

$$\int_{\mathbb{R}^3}\mathcal{F}\frac{\partial}{\partial v_i}\log\mathcal{F}_0\frac{\partial}{\partial v_i}\log\mathcal{F}_0 dv = \frac{1}{\theta^2}\int_{\mathbb{R}^3}\mathcal{F}v_i'v_i'dv = \frac{3\rho}{\theta}, \tag{A.4}$$

respectively, where integration by part and the fact that $\mathcal{F}$ and its derivatives vanish at the boundaries are employed. Therefore we get Eq. (A.1).

Appendix B. Matrix of coefficients

Applying closure (20) to the quad-FP setting, we get an explicit expression for the system (40). Let us decompose the coefficient matrix $\mathcal{L}$ into smaller blocks

$$\mathcal{L}_{9\times 9} = \left(\begin{array}{c|c|c} \mathcal{A}_{6\times 6} & \mathcal{B}_{6\times 3} \\ \hline \mathcal{C}_{3\times 6} & \mathcal{E}_{3\times 1} \\ \hline \mathcal{D}_{3\times 1} & \mathcal{G}_{3\times 1} \end{array}\right) \tag{B.1}$$

and employ the notation

$$u^{(p)}_{i_1 i_2 \dots i_n} = \int_{\mathbb{R}^3}\mathcal{F}|v'|^p v'_{i_1}v'_{i_2}\dots v'_{i_n}\,dv \tag{B.2}$$

introduced in [47]. The elements of the coefficient matrix then become

$$\mathcal{A} = \begin{pmatrix} 2u^{(0)}_{11} & 2u^{(0)}_{12} & 2u^{(0)}_{13} & 0 & 0 & 0 \\ u^{(0)}_{12} & u^{(0)}_{11}+u^{(0)}_{22} & u^{(0)}_{23} & u^{(0)}_{12} & u^{(0)}_{13} & 0 \\ u^{(0)}_{13} & u^{(0)}_{23} & u^{(0)}_{11}+u^{(0)}_{33} & 0 & u^{(0)}_{12} & u^{(0)}_{13} \\ 0 & 2u^{(0)}_{12} & 0 & 2u^{(0)}_{22} & 2u^{(0)}_{23} & 0 \\ 0 & u^{(0)}_{13} & u^{(0)}_{12} & u^{(0)}_{23} & u^{(0)}_{22}+u^{(0)}_{33} & u^{(0)}_{23} \\ 0 & 0 & 2u^{(0)}_{13} & 0 & 2u^{(0)}_{23} & 2u^{(0)}_{33} \end{pmatrix}, \tag{B.3}$$

$$\mathcal{B} = \begin{pmatrix} 2u^{(2)}_{1}+4u^{(0)}_{111} & 4u^{(0)}_{112} & 4u^{(0)}_{113} \\ u^{(2)}_{(2)}+4u^{(0)}_{112} & u^{(2)}_{1}+4u^{(0)}_{122} & 4u^{(0)}_{123} \\ u^{(2)}_{3}+4u_{113} & 4u^{(0)}_{123} & u^{(2)}_{1}+4u^{(0)}_{133} \\ 4u^{(0)}_{122} & 2u^{(2)}_{2}+4u^{(0)}_{222} & 4u^{(0)}_{223} \\ 4u^{(0)}_{123} & u^{(2)}_{3}+4u^{(0)}_{223} & u^{(2)}_{2}+4u^{(0)}_{233} \\ 4u^{(0)}_{133} & 4u^{(0)}_{233} & 2u^{(2)}_{3}+4u^{(0)}_{333} \end{pmatrix}, \tag{B.4}$$

$$\mathcal{C} = \begin{pmatrix} u^{(2)}_{1}+2u^{(0)}_{111} & u^{(2)}_{2}+4u^{(0)}_{112} & u^{(2)}_{3}+4u^{(0)}_{113} & 2u^{(0)}_{122} & 4u^{(0)}_{123} & 2u^{(0)}_{133} \\ 2u^{(0)}_{112} & u^{(2)}_{1}+4u^{(0)}_{122} & 4u^{(0)}_{123} & u^{(2)}_{2}+2u^{(1)}_{222} & u^{(2)}_{3}+4u^{(1)}_{223} & 2u^{(1)}_{233} \\ 2u^{(1)}_{113} & 4u^{(1)}_{123} & u^{(2)}_{1}+4u^{(1)}_{133} & 2u_{223} & u^{(2)}_{2}+4u^{(1)}_{233} & u^{(2)}_{3}+2u^{(1)}_{333} \end{pmatrix}, \tag{B.5}$$

$$\mathcal{D} = \begin{pmatrix} u^{(4)}-u^{(2)^2}+2u^{(2)}_{11}-2u^{(2)}u^{(0)}_{11}+6u^{(2)}_{11}-2u^{(0)}_{11}u^{(2)}-4(u^{(0)^2}_{11}+u^{(0)^2}_{12}+u^{(0)^2}_{13}) \\ 2u^{(2)}_{12}-2u^{(2)}u^{(0)}_{12}+6u^{(2)}_{12}-2u^{(0)}_{12}u^{(2)}-4(u^{(0)}_{12}u^{(0)}_{11}+u^{(0)}_{22}u^{(0)}_{12}+u^{(0)}_{13}u^{(0)}_{23}) \\ 2u^{(2)}_{13}-2u^{(2)}u^{(0)}_{13}+6u^{(2)}_{13}-2u^{(0)}_{13}u^{(2)}-4(u^{(0)}_{13}u^{(0)}_{11}+u^{(0)}_{23}u^{(0)}_{12}+u^{(0)}_{33}u^{(0)}_{13}) \end{pmatrix}, \tag{B.6}$$

$$\mathcal{E} = \begin{pmatrix} 2u^{(2)}_{12}-2u^{(2)}u^{(0)}_{12}+6u^{(2)}_{12}-2u^{(0)}_{12}u^{(2)}-4(u^{(0)}_{12}u^{(0)}_{11}+u^{(0)}_{22}u^{(0)}_{12}+u^{(0)}_{23}u^{(0)}_{13}) \\ u^{(4)}-u^{(2)^2}+2u^{(2)}_{22}-2u^{(2)}u^{(0)}_{22}+6u^{(2)}_{22}-2u^{(0)}_{22}u^{(2)}-4(u^{(0)^2}_{12}+u^{(0)^2}_{22}+u^{(0)^2}_{23}) \\ 2u^{(2)}_{13}-2u^{(2)}u^{(0)}_{13}+6u^{(2)}_{13}-2u^{(0)}_{13}u^{(2)}-4(u^{(0)}_{13}u^{(0)}_{11}+u^{(0)}_{23}u^{(0)}_{12}+u^{(0)}_{33}u^{(0)}_{13}) \end{pmatrix} \tag{B.7}$$

and

$$\mathcal{G} = \begin{pmatrix} 2u^{(2)}_{13}-2u^{(2)}u^{(0)}_{13}+6u^{(2)}_{13}-2u^{(0)}_{13}u^{(2)}-4(u^{(0)}_{13}u^{(0)}_{11}+u^{(0)}_{23}u^{(0)}_{12}+u^{(0)}_{33}u^{(0)}_{13}) \\ 2u^{(2)}_{23}-2u^{(2)}u^{(0)}_{23}+6u^{(2)}_{23}-2u^{(0)}_{23}u^{(2)}-4(u^{(0)}_{13}u^{(0)}_{12}+u^{(0)}_{23}u^{(0)}_{22}+u^{(0)}_{33}u^{(0)}_{23}) \\ u^{(4)}-u^{(2)^2}+2u^{(2)}_{33}-2u^{(2)}u^{(0)}_{33}+6u^{(2)}_{33}-2u^{(0)}_{33}u^{(2)}-4(u^{(0)^2}_{13}+u^{(0)^2}_{23}+u^{(0)^2}_{33}) \end{pmatrix}. \tag{B.8}$$

References

[1] J.L. Lebowitz, H.L. Frisch, E. Helfand, Nonequilibrium distribution functions in a fluid, Phys. Fluids 3 (3) (1960) 325–338.
[2] N.G. Van Kampen, A power series expansion of the master equation, Can. J. Phys. 39 (4) (1961) 551–567.
[3] Mohammad H. Gorji, Maniel Torrilhon, Patrick Jenny, Fokker–Planck model for computational studies of monatomic rarefied gas flows, J. Fluid Mech. 680 (2011) 574–601.
[4] Manuel Torrilhon, Modeling nonequilibrium gas flow based on moment equations, Annu. Rev. Fluid Mech. 48 (2016) 429–458.
[5] Struchtrup Henning, Manuel Torrilhon, Regularization of grad's 13 moment equations: derivation and linear analysis, Phys. Fluids 15 (9) (2003) 2668–2680.
[6] Ilya Karlin, Derivation of regularized grad's moment system from kinetic equations: modes, ghosts and non-Markov fluxes, Philos. Trans. R. Soc. A, Math. Phys. Eng. Sci. 376 (2118) (2018) 20170230.
[7] D.A. Lockerby, B. Collyer, Fundamental solutions to moment equations for the simulation of microscale gas flows, J. Fluid Mech. 806 (2016) 413–436.
[8] Graeme A. Bird, Molecular Gas Dynamics and the Direct Simulation of Gas Flows, vol. 5, Clarendon Press, Oxford, 1994.
[9] K. Nanbu, Theoretical basis of the direct simulation Monte Carlo method, in: 15th International Symposium on Rarefied Gas Dynamics, 1986, pp. 369–383.
[10] Wolfgang Wagner, A convergence proof for bird's direct simulation Monte Carlo method for the Boltzmann equation, J. Stat. Phys. 66 (3–4) (1992) 1011–1044.
[11] Michael A. Gallis, John R. Torczynski, Steven J. Plimpton, Daniel J. Rader, Timothy Koehler, Direct simulation Monte Carlo: the quest for speed, in: AIP Conference Proceedings, vol. 1628, AIP, 2014, pp. 27–36.
[12] Lowell L. Baker, Nicolas G. Hadjiconstantinou, Variance reduction for Monte Carlo solutions of the Boltzmann equation, Phys. Fluids 17 (5) (2005) 051703.
[13] Stefan K. Stefanov, On DSMC calculations of rarefied gas flows with small number of particles in cells, SIAM J. Sci. Comput. 33 (2) (2011) 677–702.
[14] Prabhu Lal Bhatnagar, Eugene P. Gross, Max Krook, A model for collision processes in gases. I. Small amplitude processes in charged and neutral one-component systems, Phys. Rev. 94 (3) (1954) 511.
[15] E.M. Shakhov, Generalization of the krook kinetic relaxation equation, Fluid Dyn. 3 (5) (1968) 95–96.
[16] Lowell H. Holway, New statistical models for kinetic theory: methods of construction, Phys. Fluids 9 (9) (1966) 1658–1673.
[17] Mieussens Luc, Discrete-velocity models and numerical schemes for the Boltzmann-bgk equation in plane and axisymmetric geometries, J. Comput. Phys. 162 (2) (2000) 429–466.
[18] Lei Wu, Craig White, Thomas J. Scanlon, Jason M. Reese, Yonghao Zhang, Deterministic numerical solutions of the Boltzmann equation using the fast spectral method, J. Comput. Phys. 250 (2013) 27–52.
[19] R.F. Pawula, Approximation of the linear Boltzmann equation by the Fokker-Planck equation, Phys. Rev. 162 (1) (1967) 186.
[20] Anatolij Vladimirovič Skorohod, Stochastic Equations for Complex Systems, vol. 13, Springer Science & Business Media, 1987.
[21] Sergei Vladimirovich Bogomolov, On Fokker-Planck model for the Boltzmann collision integral at the moderate Knudsen numbers, Math. Models Comput. Simul. 1 (6) (2009) 739.
[22] Stefan Heinz, Molecular to fluid dynamics: the consequences of stochastic molecular motion, Phys. Rev. E 70 (3) (2004) 036308.
[23] John G. Kirkwood, The statistical mechanical theory of transport processes I. General theory, J. Chem. Phys. 14 (3) (1946) 180–201.
[24] Patrick Jenny, Manuel Torrilhon, Stefan Heinz, A solution algorithm for the fluid dynamic equations based on a stochastic model for molecular motion, J. Comput. Phys. 229 (4) (2010) 1077–1098.
[25] M. Hossein Gorji, Patrick Jenny, An efficient particle Fokker–Planck algorithm for rarefied gas flows, J. Comput. Phys. 262 (2014) 325–343.
[26] M. Pfeiffer, M. Hossein Gorji, Adaptive particle–cell algorithm for Fokker–Planck based rarefied gas flow simulations, Comput. Phys. Commun. 213 (2017) 1–8.
[27] Stephan Küchlin, Patrick Jenny, Automatic mesh refinement and parallel load balancing for Fokker–Planck-DSMC algorithm, J. Comput. Phys. 363 (2018) 140–157.
[28] M. Hossein Gorji, Patrick Jenny, Fokker–Planck–DSMC algorithm for simulations of rarefied gas flows, J. Comput. Phys. 287 (2015) 110–129.
[29] Stephan Küchlin, Patrick Jenny, Parallel Fokker–Planck-DSMC algorithm for rarefied gas flow simulation in complex domains at all Knudsen numbers, J. Comput. Phys. 328 (2017) 258–277.
[30] J. Mathiaud, Luc Mieussens, A Fokker–Planck model of the Boltzmann equation with correct Prandtl number, J. Stat. Phys. 162 (2) (2016) 397–414.
[31] Fei Fei, Jing Fan, A diffusive information preservation method for small Knudsen number flows, J. Comput. Phys. 243 (2013) 179–193.
[32] S.K. Singh, Santosh Ansumali, Fokker-Planck model of hydrodynamics, Phys. Rev. E 91 (3) (2015) 033303.
[33] Eunji Jun, Marcel Pfeiffer, Luc Mieussens, M. Hossein Gorji, Comparative study between cubic and ellipsoidal Fokker–Planck kinetic models, AIAA J. (2019) 1–10.
[34] Jun Zhang, Benzi John, Marcel Pfeiffer, Fei Fei, Dongsheng Wen, Particle-based hybrid and multiscale methods for nonequilibrium gas flows, Adv. Aerodyn. 1 (1) (2019) 12.
[35] M. Hossein Gorji, Manuel Torillhon, A Fokker-Planck Model of Hard Sphere Gases Based on h-Theorem, In AIP Conference Proceedings, vol. 1786, AIP Publishing, 2016, 090001.
[36] Carlo Cercignani, The Boltzmann equation, in: The Boltzmann Equation and Its Applications, Springer, 1988, pp. 40–103.
[37] Crispin W. Gardiner, et al., Handbook of Stochastic Methods, vol. 3, Springer, Berlin, 1985.
[38] Masatoshi Shiino, Dynamical behavior of stochastic systems of infinitely many coupled nonlinear oscillators exhibiting phase transitions of mean-field type: H theorem on asymptotic approach to equilibrium and critical slowing down of order-parameter fluctuations, Phys. Rev. A 36 (5) (1987) 2393.
[39] Giovanni Sansone, Orthogonal Functions, vol. 9, Courier Corporation, 1959.
[40] Vinay Kumar Gupta, Manuel Torrilhon, Automated Boltzmann collision integrals for moment equations, in: AIP Conference Proceedings, vol. 1501, AIP, 2012, pp. 67–74.
[41] Anton Arnold, Peter Markowich, Giuseppe Toscani, Andreas Unterreiter, On convex Sobolev inequalities and the rate of convergence to equilibrium for Fokker-Planck type equations, 2001.
[42] B. Roy Frieden, Physics from Fisher information: a unification, 2000.
[43] M.T. Martin, J. Perez, A. Plastino, Fisher information and nonlinear dynamics, Phys. A, Stat. Mech. Appl. 291 (1–4) (2001) 523–532.
[44] Oksendal Bernt, Stochastic Differential Equations: An Introduction with Applications, Springer Science & Business Media, 2013.
[45] Mohammad Hossein Gorji, Fokker-Planck solution Algorithm for rarefied gas flows and applications of complex gas-surface interactions, PhD thesis, ETH, Zurich, 2014.
[46] Eunji Jun, M. Hossein Gorji, Martin Grabe, Klaus Hannemann, Assessment of the cubic Fokker–Planck–DSMC hybrid method for hypersonic rarefied flows past a cylinder, Comput. Fluids 168 (2018) 1–13.
[47] Struchtrup Henning, Macroscopic transport equations for rarefied gas flows, in: Macroscopic Transport Equations for Rarefied Gas Flows, Springer, 2005, pp. 145–160.